ARTICLES

Journal of Semiconductors
(2024) 45, 012502
doi: 10.1088/1674-4926/45/1/012502

Anisotropic etching mechanisms of 4H-SiC: Experimental and first-principles insights

Guang Yang[1, 3], Lingbo Xu[1, 3], Can Cui[1, †], Xiaodong Pi[2, 3, †], Deren Yang[2, 3], and Rong Wang[2, 3, †]

[1]Key Laboratory of Optical Field Manipulation of Zhejiang Province, Department of Physics, Zhejiang Sci-Tech University, Hangzhou 310018, China

[2]State Key Laboratory of Silicon and Advanced Semiconductor Materials & School of Materials Science and Engineering, Zhejiang University, Hangzhou 310027, China

[3]Institute of Advanced Semiconductors & Zhejiang Provincial Key Laboratory of Power Semiconductor Materials and Devices, Hangzhou Innovation Center, Zhejiang University, Hangzhou 311200, China

Abstract: Molten-alkali etching has been widely used to reveal dislocations in 4H silicon carbide (4H-SiC), which has promoted the identification and statistics of dislocation density in 4H-SiC single crystals. However, the etching mechanism of 4H-SiC is limited misunderstood. In this letter, we reveal the anisotropic etching mechanism of the Si face and C face of 4H-SiC by combining molten-KOH etching, X-ray photoelectron spectroscopy (XPS) and first-principles investigations. The activation energies for the molten-KOH etching of the C face and Si face of 4H-SiC are calculated to be 25.09 and 35.75 kcal/mol, respectively. The molten-KOH etching rate of the C face is higher than the Si face. Combining XPS analysis and first-principles calculations, we find that the molten-KOH etching of 4H-SiC is proceeded by the cycling of the oxidation of 4H-SiC by the dissolved oxygen and the removal of oxides by molten KOH. The faster etching rate of the C face is caused by the fact that the oxides on the C face are unstable, and easier to be removed with molten alkali, rather than the C face being easier to be oxidized.

Citation: G Yang, L B Xu, C Cui, X D Pi, D R Yang, and R Wang, Anisotropic etching mechanisms of 4H-SiC: Experimental and first-principles insights[J]. *J. Semicond.*, 2024, 45(1), 012502. https://doi.org/10.1088/1674-4926/45/1/012502

1. Introduction

4H silicon carbide (4H-SiC) has shown great success in high-power and high-frequency electronics, owing to its excellent properties such as a wide bandgap, high thermal conductivity, high-electron saturation velocity, and high chemical stability[1–3]. Despite the great success of 4H-SiC in electrical vehicles and photovoltaic converters, the potential of 4H-SiC in ultra-high-power electronics has not been fully addressed due to the high density of dislocations that deteriorate the device performance and exert reliability issues[4–6]. For example, dislocations have been found to increase the leakage current of 4H-SiC-based high-power devices[7, 8]. Although most of basal plane dislocations (BPDs) in 4H-SiC substrates are converted to threading edge dislocations (TEDs) during homoepitaxy, the residual BPDs in homoepitaxial 4H-SiC still trigger bipolar degradation of 4H-SiC-based bipolar devices[9, 10]. Therefore, discriminating the type of dislocations and providing accurate dislocation density is critical to the application of 4H-SiC substrates and epitaxial layers.

Molten-alkali etching has been widely used to reveal dislocations via the preferential etching of dislocations in 4H-SiC. By removing strained atoms surrounding the dislocations lines, molten-alkali etching is capable of forming characteristic etch pits of different types of dislocations in 4H-SiC. It was proposed to distinguish threading screw dislocations (TSDs), TEDs, and BPDs by the two-dimensional shape and size of etch pits. This usually needs additives to enlarge the degree of distinction among the etch pits of TSDs, TEDs, and BPDs. Taking a further step, we have found that the TSDs, threading mixed dislocations (TMDs), TEDs and BPDs can be discriminated by the incline angles to the molten-alkali-etching-induced pits[11, 12]. This facilitates the accurate statics of dislocation density in 4H-SiC. However, this approach is only effective to the (0001) Si face of 4H-SiC. The revelation of dislocations on the (000$\bar{1}$) C face usually needs higher energy approaches, such as alkali vapor etching and microwave plasma etching[13, 14]. Researchers attribute the anisotropic etching of 4H-SiC to the different activation energy between the Si face and the C face of 4H-SiC[15–17]. However, the underlying mechanism for the anisotropic etching of 4H-SiC is still ambiguous. This hinders the optimization of the etching and dislocation revealing of 4H-SiC.

In this letter, we investigate the anisotropic etching mechanism of the Si face and C face of 4H-SiC by combining molten-KOH etching, X-ray photoelectron spectroscopy (XPS) and first-principles investigations. The activation energy for the molten-KOH etching of the C face is lower than that of the Si face. The etching rate of the molten-KOH etching of the C face is higher than that of the Si face. We find that the C face shows a much higher C=O/C–O percentage (16.31%) than that of the Si face (4.8%), predicting more oxides of C existing on the C face. First-principles calculations imply the higher the oxide coverage, the more unstable the surface is. In a word, the molten-alkali etching of 4H-SiC is proceeded by the cycling of the oxidation of 4H-SiC by the dissolved oxygen and the removal of oxides by molten-alkali etching. Our

Correspondence to: C Cui, cancui@zstu.edu.cn; X D Pi, xdpi@zju.edu.cn; R Wang, rong_wang@zju.edu.cn
Received 21 JUNE 2023; Revised 21 AUGUST 2023.

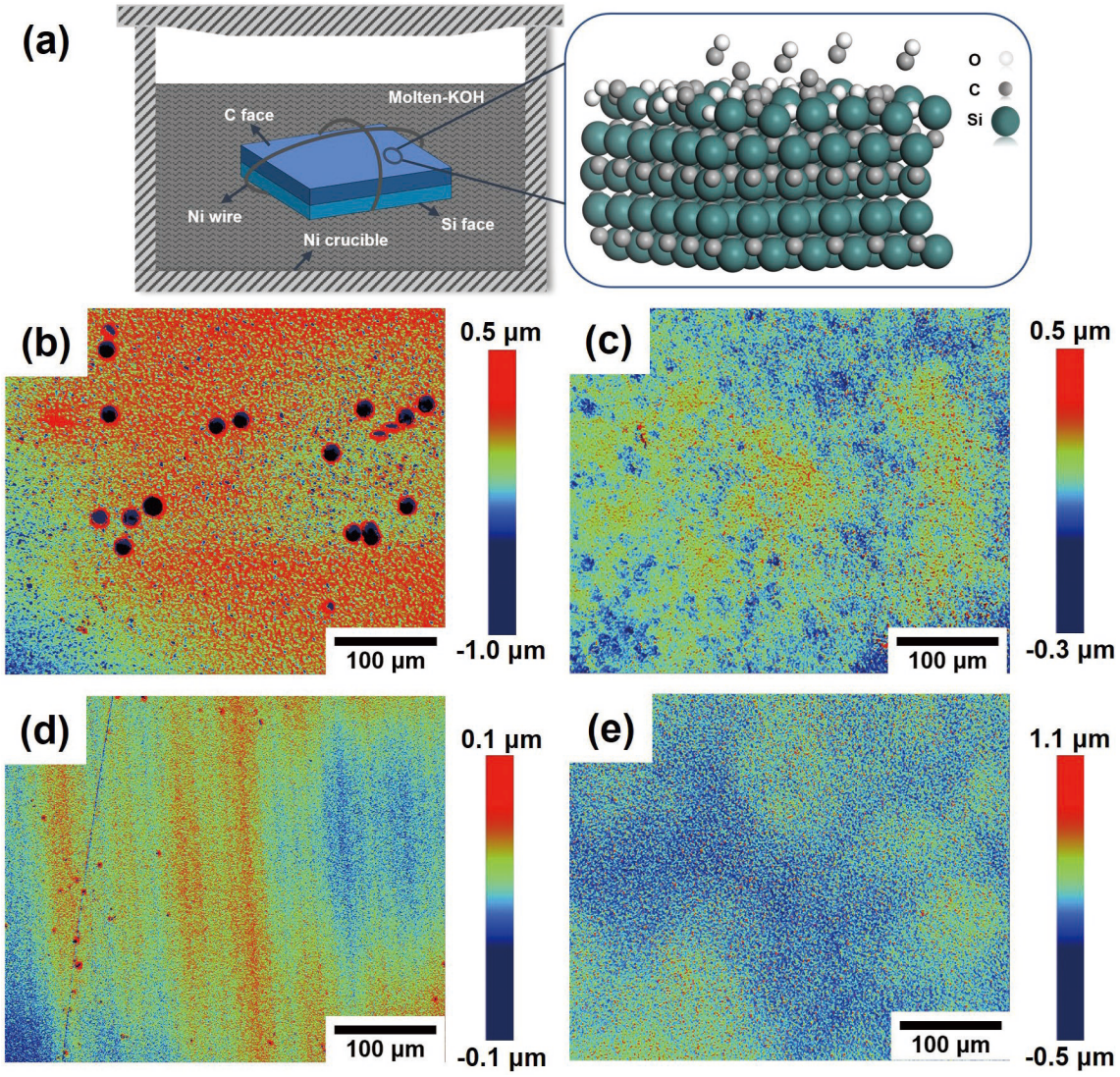

Fig. 1. (Color online) (a) Schematic diagram showing the experimental setup of molten-KOH etching, and the oxide-removal mechanism of 4H-SiC. The surface morphologies of the molten-KOH-etched 4H-SiC samples: (b) Exposed Si face, (c) protected C face, (d) protected Si face, and (e) exposed C face.

work facilitates the optimization of the molten-alkali etching conditions of 4H-SiC and paves the way for better revealing dislocations via the preferential etching of 4H-SiC.

2. Experimental section

High-purity semi-insulating (HPSI) 4H-SiC single crystals were grown by physical vapor transport (PVT) technology. The growth temperature and growth pressure were set in the range of 2200–2300 °C and 1–10 mbar, respectively. 4H-SiC wafers were sliced and mechanically polished on both sides. The wafers were cut into 20 × 20 mm^2 samples prior to molten-alkali etching. Molten-alkali etching experiments were performed at temperatures from 475 to 600 °C with the duration of 60 min in a nickel crucible. In order to measure the etching rate of the C face and Si face separately, we stacked two 4H-SiC samples together, and wrapped them tightly with a nickel wire. This exposed the Si face and C face of the top and bottom 4H-SiC sample to molten KOH, respectively [Fig. 1(a)]. After molten-KOH etching, the 4H-SiC samples were ultrasonically cleaned with deionized water and 15% hydrochloric acid solution to remove residual KOH contamination on the surface of 4H-SiC samples. The samples were then cleaned by acetone, ethanol, and finally dry with nitrogen gas. The etching rates of the Si face and C face of 4H-SiC were calculated by dividing the change of sample thickness with the etching duration.

After molten-KOH etching, the surface morphologies of the Si face and C face were observed by scanning white light interferometry (SWLI, ContourX-200, Bruker). XPS measurements were conducted with an ESCALAB Xi+ system, using an Al Kα monochromatic radiation of 1486.6 eV. The vacuum condition for the test was 2 × 10^{-10} mbar, and all the binding energies of the XPS date were calibrated with the C 1*s* peak at 284.8 eV.

3. Results and discussion

Figs. 1(b)–1(e) show the surface morphologies of the stacked 4H-SiC samples after molten-KOH etching at 475 °C. As shown in Fig. 1(b), the exposed Si face of the top 4H-SiC samples show the high density of the dislocation-related etch pits. For the protected C face of the top 4H-SiC sample and the protected Si face of the bottom 4H-SiC sample, there are almost no etch pits, indicating that the inner sides of the 4H-SiC samples are protected from being etched [Figs. 1(c) and

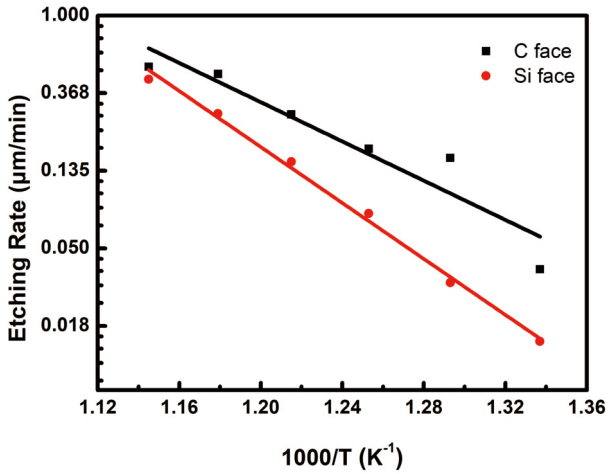

Fig. 2. (Color online) Temperature dependence of the etch rates of the Si face and C face of HPSI 4H-SiC.

1(d)]. The situation for the molten-KOH etching of the C face of the exposed bottom 4H-SiC sample has a relatively smooth surface [Fig. 1(e)]. This is caused by the isotropic etching of the C face prevailing over the preferential etching along dislocations[15].

Since the inner sides of the stacked 4H-SiC samples are protected from molten-KOH etching, we calculate the etching rates of the Si face and C face in the temperature range from 475 to 600 °C. The etching rate of the Si face and C face of 4H-SiC is calculated by dividing the material-thickness loss by the etching duration. As shown in Fig. 2, the etching rate of the C face is always higher than that of the Si face of 4H-SiC. The activation energy (E_a) is calculated by the Arrhenius fitting of the molten-KOH etching rate (E):

$$E = Ae^{-\frac{E_a}{RT}}, \quad (1)$$

where A is constant, R is the molar gas constant (8.31 J·mol^{-1}·K^{-1})[18], and T is the etching temperature. With Eq. (1), the activation energies for the molten-KOH etching of the Si face and C face of 4H-SiC are estimated to be 35.75 and 25.09 kcal/mol, respectively, which agree well with the activation energy of SiC under molten-KOH etching (32.2 kcal/mol[19]) at 450–490 °C and plasma etching (29.5 kcal/mol[13]) at 1100–1400 °C. This indicates that the C face is more vulnerable to molten-KOH etching, and the removal rate of the C face is faster than that of the Si face.

To explain the anisotropic etching of the Si face and C face, we carry out high-resolution XPS scanning on the Si face and C face of the 4H-SiC sample that is etched by molten KOH at 525 °C for 60 min. Because the distorted atoms are removed during molten-KOH etching, we calibrated all the binding energies of the XPS date with C 1*s* peak at 284.8 eV. Figs. 3(a) and 3(b) display the Si 2*p* peak of the Si face and the C face of molten-KOH etched 4H-SiC, respectively. The binding-energy peaks of the Si 2*p* of both the Si face and C face of the molten-KOH-etched 4H-SiC are located at 100.5 eV. The Si 2*p* peak can be deconvoluted into two peaks, which correspond to the characteristic peaks of the Si–C (100.4 eV) bonding and Si–O_x (101 eV) bonding[20, 21]. The binding-energy peaks of the C 1*s* spectra of the Si face of the molten-KOH-etched 4H-SiC are located at 282.6, 284.8 and 286.5 eV, which correspond to characteristic peaks of C–Si, C–C/C–H and C–O, respectively [Fig. 3(c)][22]. For the C 1*s* spectra of the C face of the molten-KOH etched 4H-SiC, the binding-energy peaks are deconvoluted into the characteristic peaks of C–Si, C–C/C–H, C–O and C=O (288.7 eV) [Fig. 3(d)]. Moreover, the C face shows a much higher C=O/C–O percentage (16.31%) than that of the Si face (4.8%). This indicates that both the Si face and C face are oxidized during the molten-KOH etching, while more oxides are on the C face due to the presence of C=O/C–O bind characteristics. Therefore, the molten-KOH etching of 4H-SiC proceeds as follows[23]:

$$SiC + 2KOH + 2O_2 \rightarrow K_2CO_3 + SiO_2 + H_2O, \quad (2)$$

$$SiC + 3K_2CO_3 \rightarrow K_2SiO_3 + 2K_2O + 4CO, \quad (3)$$

$$2KOH + SiO_2 \rightarrow K_2SiO_3 + H_2O, \quad (4)$$

$$K_2CO_3 + SiO_2 \rightarrow K_2SiO_3 + CO_2. \quad (5)$$

Since the removal of oxides by molten KOH is the same process, the anisotropic molten-KOH etching of 4H-SiC is attributed to the anisotropic oxidation of the Si face and C face of 4H-SiC. First-principle calculations are then carried out to understand the anisotropic oxidation of the Si face and C face of 4H-SiC, as implemented in the Vienna *ab* initio simulation package (VASP)[24, 25]. The projector-augmented wave (PAW) method is used to describe the electron-ion interactions[26], with the cut-off energy for the wave function expansion being 400 eV. The structural relaxations are carried out using the Perdew–Burke–Ernzerhof (PBE) exchange-correlation functional[27], until the total energy per cell and the force on each atom are converged to less than 1×10^{-8} eV and 0.01 eV/Å, respectively. Electronic structures and total energies are calculated by the screened hybrid density functional of Heyd, Scuseria, and Ernzerhof (HSE06)[28], with a 26% nonlocal Hartree–Fock exchange, to make the calculated bandgap energy of 4H-SiC consistent with the experimental bandgap energy of 4H-SiC.

We firstly investigate the most stable surface reconstruction of the Si face and C face of 4H-SiC, with the 1 × 1, 2 × 2, 3 × 3, and $\sqrt{3} \times \sqrt{3}$R30° reconstructions being considered. The surface reconstruction structures are constructed using periodic slab geometries, which consist of eight Si–C bilayers with a vacuum space of 12 Å in the *z*-axis dimension. The dangling bonds at the bottom layer are terminated by pseudo-hydrogen atoms. The atoms in the bottom three layers are fixed during structural relations to simulate the infinite solid. The Brillouin zone integration for the surface reconstructions of 1 × 1, 2 × 2, 3 × 3, and $\sqrt{3} \times \sqrt{3}$R30° are sampled with the Monkhorst–Pack scheme using a Γ-centered 10 × 10, 5 × 5, 3 × 3, and 3 × 3 special *k*-point mesh, respectively. The surface energies ΔH_{surf} of different surface reconstructions are calculated by:

$$\Delta H_{surf} = \left(E_t^{surf} - n_i\mu_i - n_H\hat{\mu}_H\right)/A_{surf}. \quad (6)$$

where E_t^{surf} is the total energy of the slab, n_i and n_H are the

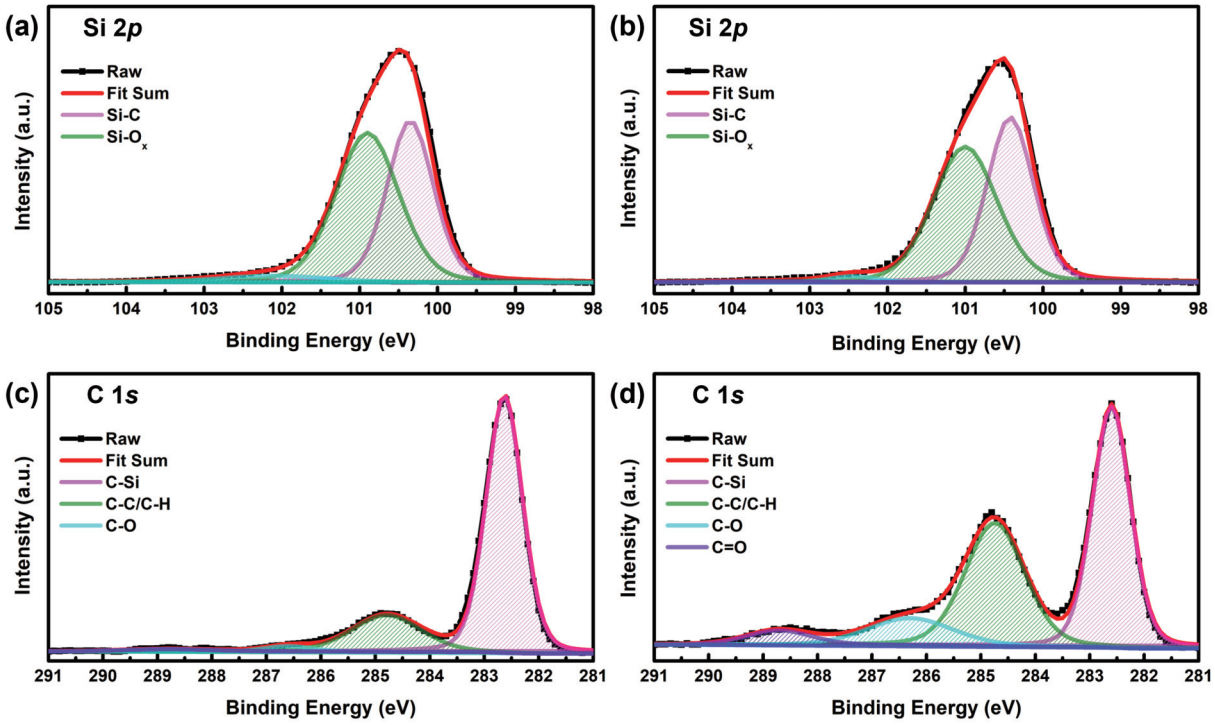

Fig. 3. (Color online) XPS high-resolution spectra of molten-KOH etched 4H-SiC wafer. (a) Si 2*p* spectrum fitting of Si face, (b) Si 2*p* spectrum fitting of the C face, (c) C 1*s* spectrum fitting of the Si face, (d) C 1*s* spectrum fitting of the C face.

number of Si/C atoms and pseudo-hydrogen atoms in the slab, μ_i and $\hat{\mu}_H$ are the chemical potentials of Si/C and pseudo-hydrogen, and A_{surf} is the area of the slab. The sum of μ_{Si} and μ_C is limited by the total energy of bulk 4H-SiC to maintain 4H-SiC in thermodynamic equilibrium. The individual values of μ_{Si} and μ_C are limited by the total energy per atom of Si and C in their bulk phases to avoid elemental precipitation. The chemical potential of pseudo-hydrogen ($\hat{\mu}_H$) is calculated by the pseudomolecule approach[29, 30]. With Eq. (6), the calculated surface energies of the surface reconstructions considered in this work are displayed in Fig. 4(a). It is clear that the surface energy of the C face is lower than that of the Si face of 4H-SiC, indicating that the C face is more stable. This is because the surface reconstructions of 1 × 1 and 3 × 3 have the lowest formation energies on the Si face and C face, respectively. Therefore, the reconstructions of 1 × 1 and 3 × 3 are the most stable reconstruction structures for the C face and Si face, respectively.

It has been proved that the oxygen locating at the bridge site has the lowest formation energy for the oxidation of the Si face and C face of 4H-SiC[31]. Therefore, we construct the bridge-site oxygen on the C face (1 × 1) and Si face (3 × 3) to investigate the anisotropic oxidation of 4H-SiC. The oxidation energies of the Si face and C face with different oxide coverages are calculated by:

$$\Delta H_{ox} = \left(E_t^{ox} - E_t^{surf} - n_O\mu_O\right)/A_{surf}, \quad (7)$$

where E_t^{ox} and E_t^{surf} are the total energies of the oxidized surface and perfect surface, n_O and μ_O are the number and chemical potential of oxygen, respectively. As shown in Fig. 4(b), the oxidation of the Si face of 4H-SiC does not cost energy, which automatically happens. For the C face of 4H-SiC, the oxidation barrier is lower than 0.1 eV/A^2, which is easy to

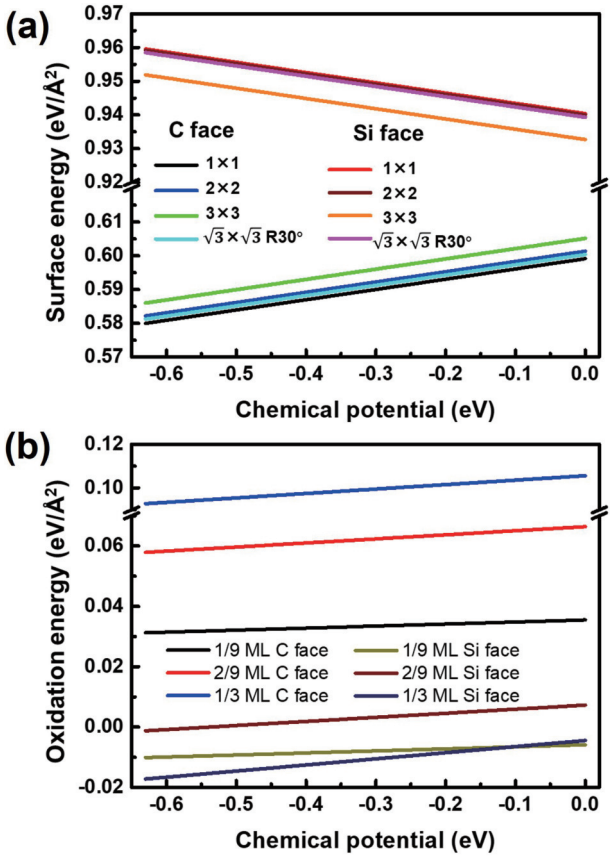

Fig. 4. (Color online) (a) Surface energies of the Si face and C face with different surface reconstructions, and (b) oxidation energies of the C face (1 × 1) and Si face (3 × 3), as functions of the chemical potential of Si.

occur. When the surface coverage of bridge-site oxygen reaches 1/3 monolayer (ML), the oxidized C face decomposes to partially oxidized surface and CO species. This indi-

cates that although the C face of 4H-SiC is more stable against oxidation, the surface of the oxidized C face becomes unstable against decomposition as the oxidation proceeds.

At last, we discuss the molten-alkali etching mechanism of 4H-SiC, as well as the anisotropic etching of the Si face and C face. The molten-alkali etching of 4H-SiC is proceeded by cycling of the oxidation of 4H-SiC by the dissolved oxygen and the removal of oxides by molten alkali. The faster etching rate of the C face is caused by the fact that the oxides on the C face are unstable, and is easier to be removed with molten alkali, compared with what happens in the Si face of 4H-SiC. This gives rise to the fast and isotropous molten-alkali etching of the C face of 4H-SiC. For the Si face of 4H-SiC, the isotropous molten-alkali etching is slower than the preferential etching of strained atoms along the dislocation lines of dislocations, which results in the revelation of dislocations on the Si face of 4H-SiC.

4. Conclusion

In conclusion, we have revealed the anisotropic etching mechanism of the Si face and C face of 4H-SiC by experimental and first-principles investigations. It has been found that the molten-alkali etching rate of the C face is faster than that of Si face. And the activation energies for the molten-KOH etching of the C face is lower than that of the Si face of 4H-SiC. Combining XPS analysis and first-principles calculations, we conclude that the molten-alkali etching of 4H-SiC is proceeded by cycling of the oxidation of 4H-SiC by the dissolved oxygen and the removal of oxides by the molten alkali. The faster etching rate of the C face is caused by the fact that the oxides on the C face are unstable and are easier to remove with molten-alkali etching, rather than the C face being easier to oxidize.

Acknowledgement

This work is supported by the Natural Science Foundation of China (Grant Nos. 62274143 & 62204216), Joint Funds of the Zhejiang Provincial Natural Science Foundation of China (Grant Nos. LHZSD24E020001) and the “Pioneer” and “Leading Goose” R&D Program of Zhejiang (Grant Nos. 2022C0102 & 2023C01010). Partial support was provided by the Leading Innovative and Entrepreneur Team Introduction Program of Hangzhou (Grant No. TD2022012), Fundamental Research Funds for the Central Universities (Grant No. 226-2022-00200), the Natural Science Foundation of China for Innovative Research Groups (Grant No. 61721005) and the Open Fund of Zhejiang Provincial Key Laboratory of Wide Bandgap Semiconductors, Hangzhou Global Scientific and Technological Innovation Center, Zhejiang University.

References

[1] Itoh A, Matsunami H. Single crystal growth of SiC and electronic devices. Crit Rev Solid State Mater Sci, 1997, 22, 111

[2] Li J J, Yang G, Liu X S, et al. Dislocations in 4H silicon carbide. J Phys D:Appl Phys, 2022, 55, 463001

[3] Yang S, Liang X W, Cui J W, et al. Impact of switching frequencies on the TID response of SiC power MOSFETs. J Semicond, 2021, 42, 082802

[4] Lebedev A A, Oganesyan G A, Kozlovski V V, et al. Radiation defects in heterostructures 3C-SiC/4H-SiC. Crystals, 2019, 9, 115

[5] Casady J B, Johnson R W. Status of silicon carbide (SiC) as a wide-bandgap semiconductor for high-temperature applications: A review. Solid State Electron, 1996, 39, 1409

[6] Kimoto T, Watanabe H. Defect engineering in SiC technology for high-voltage power devices. Appl Phys Express, 2020, 13, 120101

[7] Grekov A, Zhang Q C, Fatima H, et al. Effect of crystallographic defects on the reverse performance of 4H–SiC JBS diodes. Microelectron Reliab, 2008, 48, 1664

[8] Gao W D, Yang G, Qian Y X, et al. Dislocation-related leakage-current paths of 4H silicon carbide. Front Mater, 2023, 10, 1022878

[9] Skowronski M. Degradation of hexagonal silicon carbide-based bipolar devices. 2005 International Semiconductor Device Research Symposium, 2006, 138

[10] Song H Z, Sudarshan T S. Basal plane dislocation conversion near the epilayer/substrate interface in epitaxial growth of 4° off-axis 4H–SiC. J Cryst Growth, 2013, 371, 94

[11] Yang G, Luo H, Li J J, et al. Discrimination of dislocations in 4H-SiC by inclination angles of molten-alkali etched pits. J Semicond, 2022, 43, 122801

[12] Luo H, Li J J, Yang G, et al. Electronic and optical properties of threading dislocations in *n*-type 4H-SiC. ACS Appl Electron Mater, 2022, 4, 1678

[13] Yu J Y, Yang X L, Peng Y, et al. Revelation of the dislocations in the C-face of 4H-SiC substrates using a microwave plasma etching treatment. CrystEngComm, 2021, 23, 353

[14] Yao Y Z, Ishikawa Y, Sato K, et al. Dislocation revelation from (0001) carbon-face of 4H-SiC by using vaporized KOH at high temperature. Appl Phys Express, 2012, 5, 075601

[15] Syväjärvi M, Yakimova R, Janzén E. Anisotropic etching of SiC. J Electrochem Soc, 2000, 147, 3519

[16] Katsuno M, Ohtani N, Takahashi J, et al. Mechanism of molten KOH etching of SiC single crystals: Comparative study with thermal oxidation. Jpn J Appl Phys, 1999, 38, 4661

[17] Hatayama T, Shimizu T, Yano H, et al. Anisotropic etching of SiC in the mixed gas of chlorine and oxygen. Mater Sci Forum, 2008, 600/601/602/603, 659

[18] Segovia J J, Lozano-Martín D, Martín M C, et al. Updated determination of the molar gas constant *R* by acoustic measurements in argon at UVa-CEM. Metrologia, 2017, 54, 663

[19] Fukunaga K, Jun S D, Kimoto T. Anisotropic etching of single crystalline SiC using molten KOH for SiC bulk micromachining. Proceedings of SPIE - The International Society for Optical Engineering, San Jose, CA, US, 2006, 6109, 6109

[20] Tengeler S, Kaiser B, Chaussende D, et al. (001) 3C SiC/Ni contact interface: *in situ* XPS observation of annealing induced Ni_2Si formation and the resulting barrier height changes. Appl Surf Sci, 2017, 400, 6

[21] Wang B J, Yin J H, Chen D H, et al. Optical and surface properties of 3C–SiC thin epitaxial films grown at different temperatures on 4H–SiC substrates. Superlattices Microstruct, 2021, 156, 106960

[22] Wee A T S, Feng Z C, Hng H H, et al. Surface chemical states on 3C-SiC/Si epilayers. Appl Surf Sci, 1994, 81, 377

[23] Cui Y X, Hu X B, Xie X J, et al. Threading dislocation classification for 4H-SiC substrates using the KOH etching method. CrystEngComm, 2018, 20, 978

[24] Kresse G, Furthmüller J. Efficient iterative schemes for *ab initio* total-energy calculations using a plane-wave basis set. Phys Rev B Condens Matter, 1996, 54, 11169

[25] Kresse G, Furthmüller J. Efficiency of ab-initio total energy calculations for metals and semiconductors using a plane-wave basis set. Comput Mater Sci, 1996, 6, 15

[26] Blöchl P E. Projector augmented-wave method. Phys Rev B Condens Matter, 1994, 50, 17953

[27] Perdew J P, Burke K, Ernzerhof M. Generalized gradient approximation made simple. Phys Rev Lett, 1996, 77, 3865
[28] Heyd J, Scuseria G E, Ernzerhof M. Hybrid functionals based on a screened Coulomb potential. J Chem Phys, 2003, 118, 8207
[29] Zhang J Z, Zhang Y O, Tse K, et al. New approaches for calculating absolute surface energies of wurtzite (0001)/$(000\bar{1})$: A study of ZnO and GaN. J Appl Phys, 2016, 119, 205302
[30] Zhang Y O, Zhang J Z, Tse K, et al. Pseudo-hydrogen passivation: A novel way to calculate absolute surface energy of zinc blende (111)/$(\bar{1}\bar{1}\bar{1})$ surface. Sci Rep, 2016, 6, 20055
[31] Li W B, Zhao J J, Zhu Q Z, et al. Insight into the initial oxidation of 4H-SiC from first-principles thermodynamics. Phys Rev B, 2013, 87, 085320

Guang Yang is a master's degree student of the School of Science, Zhejiang Sci-Tech University, class of 2020. His research focuses on dislocations in 4H-SiC.

Can Cui received his PhD degree at Zhejiang University in 2006. He then carried out research at Tohoku University and National Institute for Materials Science. He is now a professor in Zhejiang Sci-Tech University. His research mainly focuses on crystal growth and optoelectronic devices.

Xiaodong Pi received his PhD degree at the University of Bath in 2004. He then carried out research at McMaster University and the University of Minnesota at Twin Cities. He joined Zhejiang University as an associate professor in 2008. He is now a professor in the State Key Laboratory of Silicon Materials, the School of Materials Science and Engineering and Zhejiang University-Hangzhou Global Scientific and Technological Innovation Center. His research mainly concerns group IV semiconductor materials and devices.

Deren Yang is an academician of the Chinese Academy of Science, presently of NingboTech University, director of the Faculty of Engineering at Zhejiang University and chief scientist of Zhejiang University-Hangzhou Global Scientific and Technological Innovation Center. He received his PhD in 1991, at Zhejiang University. In the 1990s, he worked in Japan, Germany, and Sweden for several years as a visiting researcher. He has been engaged in research on silicon materials for microelectronic devices, solar cells, and nanodevices.

Rong Wang received her PhD degree at Zhejiang University in 2014. She then carried out research at Taiyuan University of Technology and China Academy of Engineering Physics. She joined the Zhejiang University-Hangzhou Global Scientific and Technological Innovation Center in 2020. Her research mainly focuses on wide-bandgap semiconductor physics.